Afyon Kocatepe Üniversitesi Fen ve Mühendislik Bilimleri Dergisi
Afyon Kocatepe University – Journal of Science and Engineering
https://dergipark.org.tr/tr/pub/akufemubid

Araştırma Makalesi / Research Article
e-ISSN: 2149-3367
DOI: https://doi.org/10.35414/akufemubid.1526475
AKÜ FEMÜBİD 25 (2025) 021103 (279-286)
AKU J. Sci. Eng. 25 (2025) 021103 (279-286)

# Crystallographical Analysis of Martensitic Transformation Observed in Cu-Sn Alloy

*Makale Bilgisi / Article Info
Alındı/Received: 01.08.2024
Kabul/Accepted: 04.11.2024
Yayımlandı/Published: xx.xx.xxxx

## Cu-Sn Alaşımında Gözlenen Martensitik Dönüşümün Kristalografik Analizi

**Hüseyin ARSLAN***

*Kahramanmaraş Sütçü İmam Üniversitesi, Fen Fakültesi, Fizik Bölümü, Kahramanmaraş, Türkiye*



**Abstract**

Cu-Sn ingot having compositions of Cu -14.5 % at. Sn was prepared by arc melting high–purity (at least 99.9%). The ingot was annealed in an Argonne atmosphere at 1050 °C for 50 h to obtain the β-phase. The austenitic sample was cooled in liquid nitrogen and the martensite phase transformation occurred.

Using the rigorous version of the infinitesimal deformation approach in the present work, the crystallographical parameters such as habit plane normal, amount of lattice invariant shear, magnitude of the total shape deformation, orientation relationships between the austenite and martensite phase, etc. associated with Cu-Sn alloy have been predicted from a knowledge only of the lattice parameters of the austenite and final martensite phases. The lattice parameters of the austenite and martensite phases are determined from the experimental studies on Cu-Sn alloy in the present study and the crystallographic features of the martensitic transformation are compared with the values calculated using the approach. The agreement between the calculated and the observed results for this alloy system as well as the others is strong evidence for the applicability of the approach presented in this study to the cubic to the orthorhombic phase transformation observed in this alloy system.

***Keywords:*** *Martensitic Transformations; Habit Plane; Cu-Sn Alloy; Crystallography of Phase Transformations.*

**Öz**

%14,5 oranında Cu bileşimlerine sahip olan Cu-Sn külçesi. yüksek saflıkta (en az %99,9) ark eritme yoluyla hazırlandı. Külçe, β-fazını elde etmek için Argon atmosferinde 1050 °C'de 50 saat boyunca tavlandı. Martensit faz değişimi, ostenit numunenin sıvı nitrojen içerisinde soğutulmasından sonra gerçekleşti. Bu çalışmada sonsuz küçük deformasyon yaklaşımının katı versiyonunu kullanarak, habit düzlemi normali, kafes değişmez kesme miktarı, toplam şekil deformitesinin büyüklüğü, ostenit ve martensit fazı arasındaki yönelim ilişkileri vb. gibi kristalografik yönelimler ile bağlantılı Cu-Sn alaşımı yalnızca ostenit ve son martensit fazlarının kafes yönelimleri bilgisinden tahmin edilmiştir. Östenit ve martenzit fazlarının kafes yönelimleri, bu çalışmada Cu-Sn alaşımı üzerinde yapılan deneysel çalışmalardan ve martensitik dönüşümün gözlenen kristalografik özelliklerinin, yaklaşım kullanılarak hesaplanan değerlerle karşılaştırılması yoluyla belirlenmektedir. Bu alaşım sistemi için hesaplanan ve gözlemlenen sonuçlar arasındaki uyum, diğerleriyle birlikte, bu çalışmada açıklanan metodolojinin bu alaşım sisteminde gözlemlenen kübik fazdan ortorombik faz dönüşümüne uygulanabileceğine dair ikna edici kanıt sağlar.

***Anahtar Kelimeler****: Martensitik Dönüşümler;Habit Düzlemi;Cu-Sn Alaşımı; Faz Dönüşümlerinin Kristalografisi.*

## 1. Introduction

Cu-Sn alloys are one of the oldest and most important alloys known. It has found many uses in industry due to its electrical (Zhang et al. 2014) and thermal conductivity, as well as the advantages of being cheap and easy to process. There are many studies dating back to the present day investigating the different properties of the Cu-Sn alloy, especially its mechanical and thermodynamic properties (Lauro et al. 2003, Zhai et al. 2012, Hui et al. 2018, Mao et al. 2018, Ebrahimi et al. 2019, Wang et al. 2020, So et al. 2020, Karthik et al. 2021, Emadi et al. 2022, Shakarappa et al. 2023). In diffusion less phase transitions, a crystalline solid transforms from one structure to another in a process where individual atoms move less than an atomic distance relative to their nearest neighbors. A traditional approach to studying the mechanics of martensitic transformation is through the phenomenological crystallographic theory (PTMT) of martensitic transformation. This theory is well-established and has been successfully applied to numerous alloy systems (Bowles and Mackenzie 1954, Lieberman et al. 1955, Wayman 1972, Christian 2002, Nishiyama 2012). However, only a few cases demonstrate a good match between theoretical predictions and experimental results for all crystallographic parameters, which include habit plane orientations, shape deformations, and orientation relationships between the crystal lattices of

*Sorumlu Yazar / Corresponding Author: Hüseyin ARSLAN
e-posta / e-mail: arslan@ksu.edu.tr

austenite and martensite phases. Noteworthy cases involve the face-centered cubic (fcc) to body-centered tetragonal (bct) transformation with habit planes in Fe-Pt (Efsic and Wayman 1967), Fe-Ni-C (Bowles and Dunne 1969), and Fe-Al-C (Watanabe and Wayman 1971), as well as the body-centered cubic (bcc) to orthorhombic transformation in Au-Cd and Cu-Sn alloys. (Wayman 1972). A robust test of the theory involves measuring all crystallographic parameters during an ideal transformation. Recently, simpler crystallographic theories have been developed to calculate these parameters without complex numerical computations. Several researchers have successfully used these methods to derive and explain the crystallographic features. Shibata et al.'s study (Shibata-Yanagisawa and Kato 1990) is the most recent and successful example. Kato et al. employed the infinitesimal deformation (ID) approach, an approximation of the PTMT for small transformation distortions, to calculate crystallographic parameters for cubic to tetragonal transformations (Kato and Shibata-Yanagisawa 1990). While the theory and experimental results aligned well, particularly in the zirconia transformation, the small strains involved meant that comparisons between measured and calculated values of other features did not provide a stringent test of the theory.

This study aims to reformulate the rigorous version of the ID approach and apply it to the bcc to orthorhombic 9R martensitic phase transformation observed in a Cu-14.5% at. (atomic) Sn alloy. Additionally, the effects of principal distortions on crystallographic parameters, especially the habit plane, will be discussed.

The habit plane is a crystallographic plane along which atoms align during phase transformations in materials. It defines the interface between two different phases in a solid, typically in processes like martensitic transformations.

## 2. Material Method

### *2.1. Experimental*

Cu-Sn ingot having compositions of Cu -14.5 % at. Sn was prepared by arc melting high–purity (at least 99.9%). The ingot was annealed in an Argonne atmosphere at 1050 °C for 50 h to obtain the β-phase. Later the β- phased sample was cooled rapidly in water to stabilize the austenite. Then, the martensitic structure occurs immersing the austenitic sample into the liquid nitrogen.

Beta (β) phase refers to a particular phase in the phase diagram of an alloy system, typically characterized by a specific arrangement of atoms and properties. In the case of Cu-Sn (Copper-Tin) alloys, the β phase is solid and forms at certain temperature and composition ranges. It is often an intermetallic compound with a distinct crystal structure, usually body-centered cubic (BCC), although it can sometimes adopt different configurations based on the alloy system. For Cu-Sn alloys:

- β phase is stable at intermediate tin concentrations and at temperatures higher than room temperature.
- It is a solid phase, not liquid.
- The crystal structure of the β phase in the Cu-Sn system is typically body-centered cubic (BCC).

**Cu-Sn Phase Diagram**

In the Cu-Sn phase diagram, several phases, including liquid, α (solid solution), β, and γ, are observed. As the tin content increases in the alloy, different phases appear at different temperature ranges. The β phase generally forms in a specific composition and temperature range before transforming into other phases, like the α phase (FCC, face-centered cubic) or γ phase.

**Explanation Using the Cu-Sn Phase Diagram:**

1. At high temperatures (above the liquidus line), the Cu-Sn alloy is in a liquid state.
2. As it cools down, solid phases start to form, and the β phase can exist at moderate Sn concentrations (around 10-15% Sn).
3. At lower temperatures, the β phase can decompose into other phases like the α phase, depending on the alloy composition and cooling conditions.

The crystallography analysis of the alloys was performed using an x-ray diffractometer (Philips X'Pert PRO) with CuKα radiation (λ = 1.54 Å), operating at 40 kV and 30 mA. The scan was conducted in the range of 2θ = 20°-90°. Some of the x-ray diffraction patterns taken at room temperature for ingot annealed and unannealed are summarized in Figure (1 a and b) and using these figures, the lattice parameter of the B2 structure (corresponding to β or bcc structure is calculated as a0 = 2.981 $^0$A while the lattice parameters of the orthorhombic structure (martensite phase, 2H) are calculated as a = 2.685 $^0$A, b = 4.554 $^0$A and c = 4.342 $^0$A.

The equations (1) used to calculate the lattice parameters are taken from the following two studies (Armağan and Kirindi 2021, Armağan et al. 2017). The formula is;

$$a_\gamma = \frac{\lambda\sqrt{h^2l^2k^2}}{2Sin\theta_{hkl}} \quad (1)$$

where λ, (hkl), and θhkl are the wavelength of the radiation, the three Miller indices of a plane and the Bragg angle, respectively. Office excell programme was generally used in the calculations.

### *2.2. Formulation of Rigorous Version of ID Analysis*

To determine the distortion matrix $B$ that describes the lattice deformation between the initial (austenite) phase and the final (martensite) phase, the lattice correspondence and the lattice parameters of both phases must be known. This matrix can be expressed in a suitable orthonormal coordinate system, $\gamma$, which is fixed to the austenite phase. To achieve this, one of the three crystallographically equivalent lattice deformation matrices should be used.

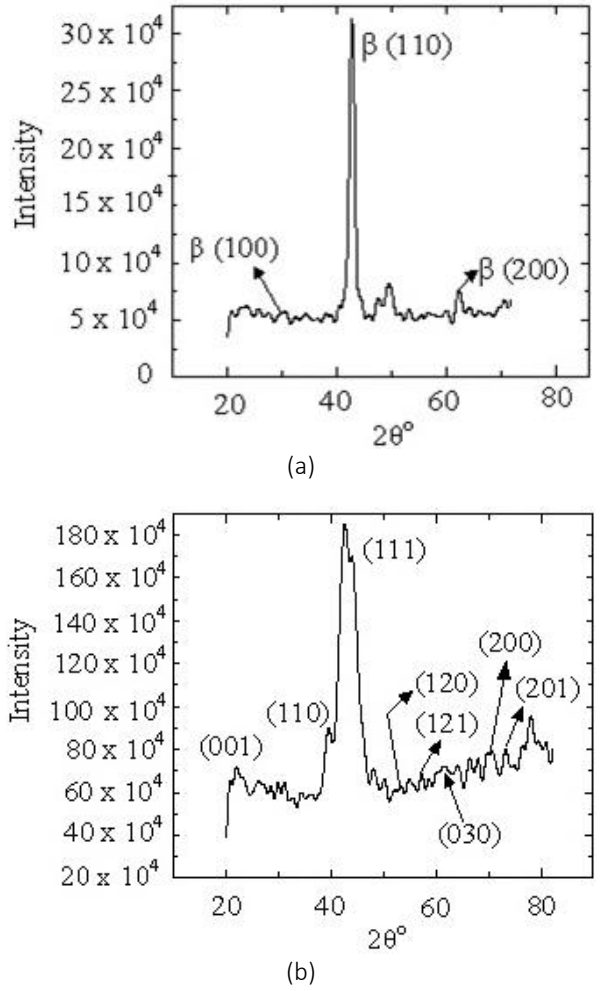


**Figure 1.** X-ray diffraction profiles of ingots (a) 0 h and (b) annealed at 1050 $^0$C for 50 h

The lattice deformation matrix, B, in the rigorous version ID approach, is generally expressed as

$$\boldsymbol{B}^{\gamma} = \begin{bmatrix} \eta_1 & 0 & 0 \\ 0 & \eta_2 & 0 \\ 0 & 0 & \eta_3 \end{bmatrix} \tag{2}$$

where $\eta_1$ and $\eta_2$ are called the principal lattice distortions and can be calculated from the lattice parameter values of the austenite and martensite phases in which the coordinate system, as is shown in Figure 1, is chosen as $x_1^{\gamma}$//[100], $x_2^{\gamma}$//[010] and $x_3^{\gamma}$//[001] According to the application of the phenomenological theory (Wayman 1972, Christian 2002, Nishiyama 2012), the (110),$[1\bar{1}0]_{\gamma}$ is slip system as lattice invariant shear system (LIS) in the Cu -14.5 % at. Sn alloy systems. In the slip system just mentioned above, the shear distortion matrix, P, can be expressed in the g coordinate system as follows.

$$\boldsymbol{P}^{\gamma} = \begin{bmatrix} 1+(m/2) & m/2 & 0 \\ -m/2 & 1-(m/2) & 0 \\ 0 & 0 & 1 \end{bmatrix} \tag{3}$$

Where m is the unknown amount of the slip deformation to be determined later. On the other hand, the total shape deformation T matrix in the rigorous version of the ID approach can be defined as follows (Murnaghan 1937, Kelly 2003, Kelly 2006, Zhang and Kelly 2009), which is known as the Lagrangian strain formula,

$$T = 1/2\ [F^{T}F - I] \tag{4}$$

Where $F^T$ is the transpose of the F matrix and so the F matrix is taken in the form

$$F = BP \tag{5}$$

So, T becomes

$$T^{\gamma} = \begin{pmatrix} T_{11}^{\gamma} & T_{12}^{\gamma} & 0 \\ T_{21}^{\gamma} & T_{22}^{\gamma} & 0 \\ 0 & 0 & T_{33}^{\gamma} \end{pmatrix} \tag{6}$$

Where

$2T_{11}^{\gamma} = \eta_1^2(1+\frac{m}{2})^2 + \eta_2^2\frac{m^2}{4} - 1, \quad 2T_{21}^{\gamma} = 2T_{12}^{\gamma} = \eta_1^2\frac{m}{2} - \eta_2^2\frac{m}{2}\left(1-\frac{m}{2}\right) \quad 2T_{22}^{\gamma} = \eta_2^2(1-\frac{m}{2})^2 + \eta_1^2\frac{m^2}{4} - 1$

and

$$2T_{33}^{\gamma} = \eta_3^2 - 1 \tag{7}$$

However, the determinant in Eq. (5) should be 0 because the determinant is an invariant variable that is independent of the preferred coordinate system. This in this instance results in two separate answers form. The only numerical solution $m_+$ = 0.201534 will be considered for a comparison with the experimental results, Bowles-Mackenzie (B-M) theory, and ID methodology since this amount of slip is much more reasonable than the other.

### *2.3. Determination of Habit Plane*

The coordinate system is fixed to the parent phase and the *n* coordinate system with its $x_3^n$ axis perpendicular to

the habit plane can be related to the parent coordinate system by direction cosines, as defined in Table 1 with two angles. The mutually perpendicular $x_1^n$ and $x_2^n$ axes can be chosen arbitrarily, provided they are both perpendicular to the $x_3^n$ axis (see Fig. 2).

Table 1. The definition of direction cosines aij between axis and axis.

| $\gamma$ \ $n$ | $x_1^n$ | $x_2^n$ | $x_3^n$ |
|---|---|---|---|
| $x_1^\gamma$//[100]$_\gamma$ | $\cos\theta\cos\phi$ ($a_{11}$) | $-\sin\phi$ ($a_{12}$) | $\sin\theta\cos\phi$ ($a_{13}$) |
| $x_2^\gamma$//[010]$_\gamma$ | $\cos\theta\sin\phi$ ($a_{21}$) | $\cos\phi$ ($a_{22}$) | $\sin\theta\sin\phi$ ($a_{23}$) |
| $x_3^\gamma$//[001]$_\gamma$ | $-\sin\theta$ ($a_{31}$) | 0 ($a_{32}$) | $\cos\theta$ ($a_{33}$) |

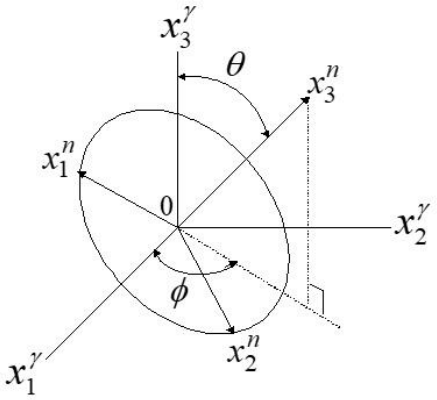


**Figure 2.** The relationship between the coordinate system ($x_j^n$) and the substrate coordinate system ($x_i^\gamma$).

The matrix $T^\gamma$, expressed in the parent coordinate system, can be converted into the matrix $T^n$ expressed in the *n* coordinate system through standard tensor conversion. In this case, becomes by the usual tensor conversion. In this case, $T^n$ becomes

$$\boldsymbol{T}_{ij}^n = \sum_{k=1}^3 \sum_{l=1}^3 a_{ki} a_{lj} \boldsymbol{T}_{kl}^\gamma \quad (8)$$

Here, n indicates that the matrix is described in the $X_1^n$ - $X_{12}^n$ - $X_{31}^n$ orthonormal coordinate system with a plane parallel to the invariant plane, i.e., the habit plane. Some researchers (Wayman 1972) have performed elasticity calculations to demonstrate that the elastic strain energy is minimized to be zero From Eq. (7), the following invariant plane deformation condition (IPS) can be derived:

$$\boldsymbol{T}_{11}^n = \boldsymbol{T}_{12}^n = \boldsymbol{T}_{22}^n = 0 \quad (9)$$

This condition implies that the elastic energy associated with the formation of the martensitic phase is zero. In other words, the formation of the martensitic phase does not require any energy expenditure (Khachaturyan and Shatalov 1969, Mura et al. 1976). Solving these equations in Eq. (8) simultaneously and using Table 1, the unknown two parameters such as q and f determining the habit plane direction can be found easily as a function of the lattice parameters of the initial and final phase only:

$$P_h = [\cos\theta, \sin\theta \sin\varphi, \sin\theta \cos\varphi] \quad (10)$$

$$tan\,\varphi = \frac{T_{12}^\gamma}{T_{11}^\gamma}\left[1 \mp \sqrt{1 + \frac{T_{11}^\gamma T_{22}^\gamma}{(T_{12}^\gamma)^2}}\right] \quad (11)$$

and

$$tan\,\theta = cos\,\varphi \sqrt{-\frac{T_{22}^\gamma tan^2\varphi + 2T_{12}^\gamma tan\,\varphi + T_{11}^\gamma}{T_{33}^\gamma}} \quad (12)$$

The numerical values of the crystallographical parameters calculated in the present study for the two values m, which are crystallographical is independent of each other, are listed in Table 2.

Table 2. The measured lattice parameter of the austenite and martensite phases for Cu -14.5 % at. Sn alloy

| Alloy | Lattice parameter, $^0$A (Arslan 2014) | | Principal strains |
|---|---|---|---|
| | Austenite Phase:$a_0$ | Martensite Phase: a,b,c | $\eta_1$ $\eta_2$ $\eta_3$ |
| Cu -14.5 % at. Sn | 2.981 | 2.685, 4.554, 4.342 | 0.900704, 1.08023, 1.029942 |

Unless we find the component of the rotation matrix, it is impossible to discuss the orientation relationship between the initial and final phases. Since the orientation relationship between the austenite phase and martensite phase are determined only by elements of the rotation matrix, R, rigid body rotation is not repeated here. The details for obtaining it can be found in some graduate books (Wayman 1972, Christian 2002, Nishiyama 2012).

**3. Results**

It is concluded from the diffraction patterns in Figure (1) that the martensite structure has an orthorhombic structure. The lattice parameter's values related to β austenite and orthorhombic martensite phase, which are measured from the diffraction patterns, are relisted in Table 2 (Kennon and Bobowles 1969, Kennon 1972, Pandey et al. 1991). Using lattice parameter values, $\eta_1$ and $\eta_2$ can be determined from the following equations:

$$\eta_1 = \frac{a}{a_0} \quad \text{and} \quad \eta_2 = \frac{b}{\sqrt{2}a_0} \quad \text{and} \quad \eta_3 = \frac{c}{\sqrt{2}a_0} \quad (13)$$

Using Eq. (13), after determining the values of principal misinterpretations related to phase transformation in the Cu -14.5 % at. Sn alloy, these values are given in Table 3. Conversely, the orientation relationship between the austenite and martensite phases, the amount of the lattice invariant shear, and the habit plane normal are similarly obtained analytically. Table 4 also lists the numerical values of the corresponding

crystallographic criteria to those obtained from the PTMT, such as Bowles-Mackenzie (B-M) theory, ID methodology, and together with the available experimental results, to compare the computational results with those obtained using the strict version of ID methodology. To metallographically investigation, an SEM micrograph of the alloy is taken.

**Table 3.** The crystallographic results for the slip as LIS in a Cu - 14.5 % at. Sn alloy in the present study. The calculations were performed for the $(110)_\gamma$ $[\bar{1}10]_\gamma$ slip system in the transformation bcc phase to the orthorhombic phase.

| Crystallographic criterions | $m_+$=0.201534 | $m_-$=0.158019 |
|---|---|---|
| Habit plane, $P_h$ | $\begin{bmatrix}0.21236\\0.649827\\0.729814\end{bmatrix}$ | $\begin{bmatrix}0.649689\\0.212781\\0.729814\end{bmatrix}$ |
| Direction of total shape deformity, $d_T$ | $\begin{bmatrix}-0.21874\\-0.66927\\0.71009\end{bmatrix}$ | $\begin{bmatrix}-0.669265\\-0.218776\\0.710086\end{bmatrix}$ |
| The magnitude of total shape deformity, $m_T$ | 0.056971 | 0.056974 |
| Orientation relationships | | |
| $[\bar{1}01]_\gamma - [100]_\alpha$ | $2.01^0$ | $3.17^0$ |
| $[0\bar{1}0]_\gamma - [010]_\alpha$ | $1.62^0$ | $0.68^0$ |
| $[\bar{5}04]_\gamma - [001]_\alpha$ | $0.74^0$ | $0.04^0$ |
| $(101)_\gamma - (001)_\alpha$ | $0.86^0$ | $0.02^0$ |

Figure 3 shows a surface shot of three neighboring austenite phase grains with a banded substructure, starting from grain borders at 600 $^0$C. Therefore, in the present study, the numerical solutions in reference (Wayman 1972) with those obtained using the strict version of ID methodology are compared, because the numerical values determined in this study seem to coincide with those of this reference when we first glance at experimental results. In the present study, the numerical solutions in reference (Pandey et al. 1991) with those obtained using the strict version of ID methodology are compared, because the numerical values determined in this study are in agreement with those of this reference.

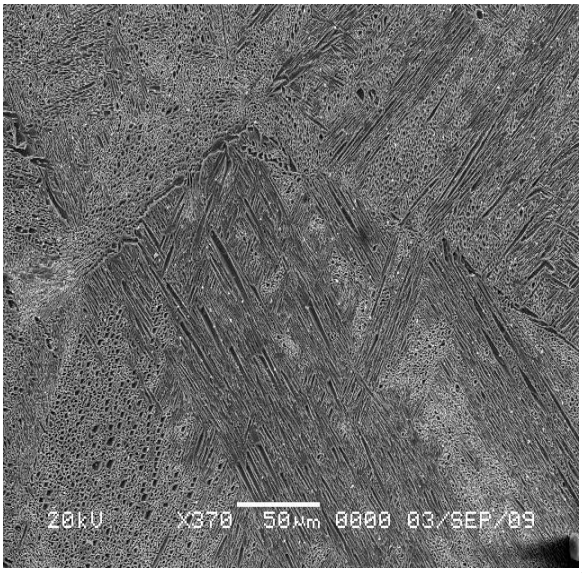


**Figure 3.** SEM micrograph of the sample annealed at 600 $^o$C viewed at room temperature**.**

As can be seen from Tables (3) and (4), the agreement between B-M theory and the strict version of ID methodology is found to be excellent. The orientation of the habit plane between the strict version of ID methodology and B-M theory differs by nearly 4.440 while this difference for B-M theory - experimental result is nearly 6.60 and for the strict version of ID methodology- experimental result is nearly 2.20. Whereas the habit plane orientation determined from the ID methodology differs by nearly 12.630 concerning that obtained using the strict version of the ID methodology. This difference originated from the fact that ID methodology neglects the second and higher-order terms of the lattice misinterpretation. It is concluded from the point of habit $A = \pi r^2$plane orientation view that this approach is better than the ID methodology.

**Table 4.** For a solution m = 0.201534 in Cu -14.5 % at. Sn alloy, a comparison of the numerical solutions among the strict version of the ID methodology treated in this study, usual B-M theory, ID methodology, and experimental results (Arslan 2014).

| Crystallographic criterions | Present theoretical study | ID approach | B-M theory | Experimental |
|---|---|---|---|---|
| The magnitude of the total shape deformity, $m_T$ | 0.0567 | 0.049 | 0.119 | 0.109 |
| Habit plane | $\begin{bmatrix}0.21236\\0.649827\\0.729814\end{bmatrix}$ | $\begin{bmatrix}0\\0.623728\\0.781641\end{bmatrix}$ | $\begin{bmatrix}-0.2862\\0.6270\\0.7245\end{bmatrix}$ | $\begin{bmatrix}-0.1786\\0.6657\\0.7246\end{bmatrix}$ |
| Direction of total shape deformity, dT | $\begin{bmatrix}-0.21874\\-0.66927\\0.71009\end{bmatrix}$ | $\begin{bmatrix}0\\-0.62373\\0.781641\end{bmatrix}$ | $\begin{bmatrix}-0.1781\\-0.7668\\0.6166\end{bmatrix}$ | $\begin{bmatrix}-0.1093\\-0.7897\\0.6037\end{bmatrix}$ |
| Orientation relationships | | | | |

| | | | | |
|---|---|---|---|---|
| $[\bar{1}01]_\gamma - [100]_\alpha$ | $2.01^0$ | $0.93^0$ | - | $5.80^0$ |
| $[0\bar{1}0]_\gamma - [010]_\alpha$ | $1.62^0$ | $1.11^0$ | - | $4.60^0$ |
| $[\bar{5}04]_\gamma - [001]_\alpha$ | $0.74^0$ | $3.18^0$ | - | $4.00^0$ |
| $(101)_\gamma - (001)_\alpha$ | $0.86^0$ | $3.24^0$ | $0^0$ | - |

On the other hand, there is no difference between the strict version of ID methodology and B-M theory in the magnitude of the total shape deformity. The difference between the strict version of ID methodology and experimental results is at almost 0.052 while the value corresponding to the difference between the strict version of ID methodology and B-M theory is only 0.062. The results obtained from the strict version of ID methodology are generally in agreement with those calculated from the B-M theory and also with the experimental observations, but especially from the point of the habit plane view, the theoretical analysis in the present study does not confirm that obtained from the ID methodology because the absolute values of the principal misinterpretations related to the martensitic transformation in the ID methodology have small values. For this purpose, the calculations treated in the present study were carried out in zirconia alloy in which the principal misinterpretations were very small, and the obtained results are shown in Table 5.

Table 5. For a solution f- = 0.201534 in zirconia alloy, a comparison of the numerical solutions among the strict version of the ID methodology treated in this study, usual WLR theory (Wayman 1972, Christian 2002, Nishiyama 2012) and ID methodology (Shibata-Yanagisawa and Kato 1990).

| Crystallographic criterions | Present study | ID approach | WLR Theory |
|---|---|---|---|
| Volume fraction, f- | 0.406822 | 0.4048 | 0.4068 |
| Magnitude of the total shape deformity, $m_T$ | 0.009716 | 0.009752 | 0.009688 |
| Habit plane | $\begin{bmatrix}-0.82674\\-0.01191\\0.5662465\end{bmatrix}$ | $\begin{bmatrix}0.8247\\0.5656\\0\end{bmatrix}$ | $\begin{bmatrix}0.8267\\0.5625\\-0.0118\end{bmatrix}$ |
| Direction of total shape deformity, $d_T$ | $\begin{bmatrix}0.828621\\-0.00854\\0.559745\end{bmatrix}$ | $\begin{bmatrix}-0.8247\\0.5656\\0\end{bmatrix}$ | $\begin{bmatrix}-0.8293\\0.5587\\-0.0119\end{bmatrix}$ |
| Orientation relationships | | | |
| $[100]_\gamma - [100]_\alpha$ | $0.26^0$ | $0.26^0$ | $0.26^0$ |
| $[010]_\gamma - [010]_\alpha$ | $0^0$ | $0.62^0$ | $0.61^0$ |
| $[001]_\gamma - [001]_\alpha$ | $0.26^0$ | $0.56^0$ | $0.56^0$ |
| $(101)_\gamma - (001)_\alpha$ | $0.86^0$ | $3.24^0$ | $0^0$ |

Here, in the martensitic transformation from cubic phase to tetragonal phase, the slip system as LIS is (011) $[1\bar{1}0]_\gamma$The lattice parameter in this alloy are $a_0$ = 0.5127 nm (austenite) a= 0.5093 nm and c= 0.5177 nm (martensite). The principal misinterpretations are calculated as $\eta_1=\eta_2=a/a_0=0.993368$ and $\eta_3=c/a_0=1.009752$. It can be seen from Table 5 for a comparison of the results of the strict version of ID methodology with those of ID methodology that there is no meaningful difference in the habit plane orientation and direction of the shape deformity. The difference between these two approaches concerning the habit plane orientation and direction of the shape deformity is % 0.0036 0 i. e. nearly zero. For relationships, on the other hand, there are good agreements among the three theories.

## 4. Discussion and Conclusion

In this study, the observed crystallographic properties of the martensitic transformation were calculated using the approach for the Cu -14.5 % at. Sn alloy systems were determined by comparing them with the values obtained from the experimental studies.

The agreement between the calculated and observed results for this alloy system provides strong evidence that the methodology described in this work is applicable to the cubic to orthorhombic phase transformation observed in this alloy system.

The suitability of the chosen methodology can be seen from the fact that the results are very close to each other and are also in harmony with the experimental results.

It is hoped and believed that this study will guide and open new horizons for young scientists who will study this subject in the future

**Declaration of Ethical Code**

In this study, we ensure compliance with all the rules outlined in the "Higher Education Institutions Scientific Research and Publication Ethics Directive," and confirm that none of the actions listed under the "Actions Against Scientific Research and Publication Ethics" have been committed.

**Declaration of Competing Interest**

The authors have no conflicts of interest to declare regarding the content of this article.

**Data Availability Statement**

All data generated or analyzed during this study are included in this published article.

## References


Armağan, O., Kırındı T. 2021. Effect of Mn ammount on phase transformations and magnetic properties in Fe-Mn-Mo-Si alloys. *Archives of Metallurgy and Materials,* **66(1)**, 259-266. https://doi.org/10.24425/amm.2021.134783

Armağan, O., Sarı, U., Çağrı, Y., Kırındı T. 2017. Effects of thermal and deformation on martensitic transformation and magnetic properties in Fe-17%Mn-4.5%X (X = Co and Mo) alloys. *Micron*, **103**, 34-44. https://doi.org/10.1016/j.micron.2017.09.007

Arslan, H. 2014. Structural Evolution Properties of Cu-25 wt %Sn Alloy During Ball Milling. *Journal of Advanced Thermal Science Research*, **1**(**1**), 25–31. http://dx.doi.org/10.15377/2409-5826.2014.01.01.4

Bowles, J., Dunne, D. 1969. The role of plastic accommodation in the (225) martensite transformation. *Acta Metallurgica*, **17**, 677–685. https://doi.org/10.1016/0001-6160(69)90128-X

Bowles, J., Mackenzie, J. 1954. The crystallography of martensite transformations III. Face-centred cubic to body-centred tetragonal transformations. *Acta Metallurgica*, **2**, 224–234. https://doi.org/10.1016/0001-6160(54)90102-9

Christian, J.W. 2002. Characteristics of Martensitic Transformations. *The Theory of Transformations in Metals and Alloys*, 961–991. Pergamon Oxford.

Ebrahimi, M., Attarilar, S., Shaeri, M.H., Gode, C., Armoon, H., Djavanroodi, F. 2019. An investigation into the effect of alloying elements on corrosion behavior of severely deformed Cu-Sn alloys by equal channel angular pressing. *Archives of Civil and Mechanical Engineering*, **19**, 842–850. https://doi.org/10.1016/j.acme.2019.03.009

Efsic, E.J., Wayman, C.M. 1967. Crystallography of the fcc to bcc martensitic transformation in an iron-platinum alloy. *AIME Met. Soc. Trans*, **239**, 873–882.

Emadi, F., Vuorinen, V., Mertin, S., Widell, K., Paulasto-Kröckel, M. 2022. Microstructural and mechanical characterization of Cu/Sn SLID bonding utilizing Co as contact metallization layer. *Journal of Alloys and Compounds*, **929**, 167228. https://doi.org/10.1016/j.jallcom.2022.167228

Hui, J., Feng, Z., Fan, W., Yuan, X. 2018. The influence of power spinning and annealing temperature on microstructures and properties of Cu-Sn alloy. *Materials Characterization*, **144**, 611–620. https://doi.org/10.1016/j.matchar.2018.08.015

Karthik, M., Abhinav, J., Shankar, K. V. 2021. Morphological and Mechanical Behaviour of Cu–Sn Alloys—A review. *Metals and Materials International*, **27**, 1915–1946. https://doi.org/10.1007/s12540-020-00899-z

Kato, M., Shibata-Yanagisawa, M. 1990. Infinitesimal deformity approach of the phenomenological crystallographic theory of martensitic transformations. *Journal of Materials Science*, **25**, 194–202. https://doi.org/10.1007/BF00544207

Kelly, P.M. 2003. Martensite crystallography—the apparent controversy between the infinitesimal deformity approach and the phenomenological theory of martensitic transformations. *Metallurgical and Materials Transactions A*, **34**, 1783–1786. https://doi.org/10.1007/s11661-003-0144-7

Kelly, P.M. 2006. Martensite crystallography—The role of the shape strain. *Materials Science and Engineering: A*, **438**, 43–47. https://doi.org/10.1016/j.msea.2006.02.065

Kennon, N. 1972. The complementary strain for the b.c.c. to orthorhombic martensite transformation in Cu-Sn alloys. *Acta Metallurgica*, **20**, 5–10. https://doi.org/10.1016/0001-6160(72)90107-1

Kennon, N., Bowles, J. 1969. The crystallography of the B.C.C. to orthorhombic γ'1 martensite transformation in copper-tin alloys. *Acta Metallurgica*, **17**, 373–380. https://doi.org/10.1016/0001-6160(69)90017-0

Khachaturyan, A.G., Shatalov, G.A. 1969. Theory of Macroscopic Periodicity for a Phase Transition in the Solid State. *Journal of Experimental and Theoretical Physics*, **29**(**3**), 557-561.

Lauro, P., Kang, S.K., Choi, W.K., Shih, D.-Y. 2003. Effects of mechanical deformity and annealing on the microstructure and hardness of Pb-free solders. *Journal of Electronic Materials*, **32**, 1432–1440. https://doi.org/10.1007/s11664-003-0112-4

Lieberman, D.S., Wechsler, M.S., Read, T.A. 1955. Cubic to orthorhombic diffusionless phase change - Experimental and theoretical studies of AuCd. *Journal of Applied Physics*, **26**, 473–484. https://doi.org/10.1063/1.1722021

Mao, Z., Zhang, D.Z., Jiang, J., Fu, G., Zhang, P. 2018. Processing optimisation, mechanical properties and microstructural evolution during selective laser melting of Cu-15Sn high-tin bronze. *Materials Science and Engineering: A*, **721**, 125–134. https://doi.org/10.1016/j.msea.2018.02.051

Mura, T., Mori, T., Kato, M. 1976. The elastic field caused by a general ellipsoidal inclusion and the application to martensite formation. *Journal of the Mechanics and Physics of Solids*, **24**(**5**), 305–318. https://doi.org/10.1016/0022-5096(76)90028-4

Murnaghan, F. D. 1937. Finite deformations of an elastic solid. *American Journal of Mathematics*, **59**(**2**), 235-260.

Nishiyama, Z. 2012. Martensitic transformation. *Elsevier, Academic press Inc.* Edited by Morris E. Fine, M. Meshii, C.M. Wayman. London.

Pandey, D., Ojha, S.N., Tiwari, R.S. 1991. Martensitic transformation in Cu–Sn alloys. *Phase Transitions*, **35**, 1–26. https://doi.org/10.1080/01411599108205203

Shakarappa, R., Arul Peter, A., Mallikarjuna, M.V., Padmanabhan, S., Rathna Kumar, P. 2023. Influence of aluminium oxide and graphene on the mechanical properties of Cu-Sn alloy composites. *Materials Today: Proceedings*, **92**, 880–885. https://doi.org/10.1016/j.matpr.2023.04.458

Shibata-Yanagisawa, M., Kato, M. 1990. Crystallographic Analysis of Cubic (Tetragonal) to Monoclinic Martensitic Transformations based on the Infinitesimal Deformity Approach. *Materials Transactions, JIM*, **31**, 18–24. https://doi.org/10.2320/matertrans1989.31.18

So, S.-M., Kim, K.-Y., Lee, S.-J., Yu, Y.-J., Lim, H.-A., Oh, M.-S. 2020. Effects of Sn content and hot deformity on microstructure and mechanical properties of binary high Sn content Cu–Sn alloys. *Materials Science and Engineering: A*, **796**, 140054. https://doi.org/10.1016/j.msea.2020.140054

Watanabe, M., Wayman, C.M. 1971. Crystallography of the martensite transformation in Fe−Al−C alloys. *Metallurgical Transactions*, **2**, 2229–2236. https://doi.org/10.1007/BF02917555

Wayman, C.M. 1972. Crystallographic theories of martensitic transformations. *Journal of the Less Common Metals*, **28**, 97–105. https://doi.org/10.1016/0022-5088(72)90172-5

Wang, Q., Zhou, R., Li, Y., Geng, B. 2020. Characteristics of dynamic recrystallization in semi-solid CuSn10P1 alloy during hot deformity. *Materials Characterization*, **159**, 109996. https://doi.org/10.1016/j.matchar.2019.109996

Zhang, J., Cui, X., Wang, Y., Yang, Y., Lin, J. 2014. Characteristics of ultrahigh electrical conductivity for Cu–Sn alloys. *Materials Science Technology*, **30**, 506–509. https://doi.org/10.1179/1743284713Y.0000000370

Zhang, M.X., Kelly, P.M. 2009. Crystallographic features of phase transformations in solids. *Progress in Materials Science*, **54**, 1101–1170. https://doi.org/10.1016/j.pmatsci.2009.06.001

Zhai, W., Wang, W.L., Geng, D.L., Wei, B. 2012. A DSC analysis of thermodynamic properties and solidification characteristics for binary Cu-Sn alloys. *Acta Materialia*, **60**, 6518–6527. https://doi.org/10.1016/j.actamat.2012.08.013